

Experiments and FE modeling of stress–strain state in ReBCO tape under tensile, torsional and transverse load

This content has been downloaded from IOPscience. Please scroll down to see the full text.

2015 Supercond. Sci. Technol. 28 055006

(<http://iopscience.iop.org/0953-2048/28/5/055006>)

View [the table of contents for this issue](#), or go to the [journal homepage](#) for more

Download details:

IP Address: 130.89.45.232

This content was downloaded on 23/12/2015 at 13:08

Please note that [terms and conditions apply](#).

Experiments and FE modeling of stress–strain state in ReBCO tape under tensile, torsional and transverse load

K Ilin¹, K A Yagotintsev¹, C Zhou¹, P Gao¹, J Kosse¹, S J Otten¹,
W A J Wessel¹, T J Haugan², D C van der Laan³ and A Nijhuis¹

¹ University of Twente, Faculty of Science & Technology, 7522 NB Enschede, The Netherlands

² US Air Force Research Laboratory, Wright Patterson AFB, OH 45433, USA

³ Advanced Conductor Technologies and University of Colorado, Boulder, CO 80301, USA

Received 9 December 2014

Accepted for publication 25 February 2015

Published 24 March 2015



CrossMark

Abstract

For high current superconductors in high magnet fields with currents in the order of 50 kA, single ReBCO coated conductors must be assembled in a cable. The geometry of such a cable is mostly such that combined torsion, axial and transverse loading states are anticipated in the tapes and tape joints. The resulting strain distribution, caused by different thermal contraction and electromagnetic forces, will affect the critical current of the tapes. Tape performance when subjected to torsion, tensile and transverse loading is the key to understanding limitations for the composite cable performance. The individual tape material components can be deformed, not only elastically but also plastically under these loads. A set of experimental setups, as well as a convenient and accurate method of stress–strain state modeling based on the finite element method have been developed. Systematic measurements on single ReBCO tapes are carried out combining axial tension and torsion as well as transverse loading. Then the behavior of a single tape subjected to the various applied loads is simulated in the model. This paper presents the results of experimental tests and detailed FE modeling of the 3D stress–strain state in a single ReBCO tape under different loads, taking into account the temperature dependence and the elastic-plastic properties of the tape materials, starting from the initial tape processing conditions during its manufacture up to magnet operating conditions. Furthermore a comparison of the simulations with experiments is presented with special attention for the critical force, the threshold where the tape performance becomes irreversibly degraded. We verified the influence of tape surface profile non-uniformity and copper stabilizer thickness on the critical force. The FE models appear to describe the tape experiments adequately and can thus be used as a solid basis for optimization of various cabling concepts.

Keywords: HTS, superconductivity, coated conductor, finite element method, numerical simulation, mechanical load

(Some figures may appear in colour only in the online journal)

1. Introduction

Industrial application of high temperature superconductors (HTSs) requires high current densities and in case low inductances are required, e.g. for fusion or accelerator magnets, HTS tapes need to be assembled in a suitable cable geometry. Several cabling methods were suggested for HTS tapes like conductor on round core (CORC) [1], twisted

stacked-tape [2] and Roebel cable [3] to assemble high current HTS cables. Tapes in those cables are subjected to tensile, torsional and transverse loads introduced during cable manufacture, by thermal contraction of the tape materials from cool-down and eventually by electromagnetic forces during operation. These loads affect the strain state of the ReBCO layer and hence the conductor critical current. If the load exceeds a certain limit (irreversibility strain limit) crack

formation is initiated in the ReBCO layer, which causes an irreversible degradation of the conductor.

The aim of this work is to build a tape model, based on experimentally verified material properties and predict the critical loads coinciding with irreversible behavior, i.e. permanently degrading critical current (I_c). The analytical analysis of a single tape performance as a part of a cable is complex because the various tape components are deformed both elastically and plastically under these loads. We use a FE model to numerically simulate the strain in the superconducting layer of SuperPower[®] 2G HTS tape SCS4050 tape [4] under the various applied loads. We use commercial ABAQUS software to model the tape. Direct integration method (ABAQUS/Standard) and static type of analysis was used. We validate the model by single tape experimental measurements that include tape critical current behavior under transverse, tensile and torsional loads.

After completion of the single tape model and verification via the prediction of the stress–strain state of single tape under various loads and the corresponding degradation of the critical current, a solid basis is provided to simulate and optimize the design of any cable, and predict the critical strain level of the tape under cabled conditions.

All models and experiments were performed using SuperPower[®] SCS4050 [4]. As revealed by Osamura *et al* [5], when SCS4050 tape is subjected to 0.7% of axial applied tensile strain, cracks are initiated in the ReBCO layer. At that point the intrinsic strain in the ReBCO layer becomes 0.45% (irreversibility strain), the difference is caused by compressive strain in the ReBCO layer due to different thermal contraction coefficients of the tape components from tape production process to eventually 77 K. In this paper we consider the start of irreversible degradation of the critical current at the instant when the intrinsic strain in the ReBCO layer reaches 0.45% tensile strain. We call the load on the tape that corresponds to the irreversibility strain in the ReBCO layer the ‘critical load’.

2. Experimental facilities

2.1. Uni-axial tensile stress–strain setup

Several tape samples are tested in the stress–strain testing rig to determine the mechanical axial tensile stress–strain characteristic (without transport current). The obtained stress–strain data also serve as an input for the torsion–tensile tape measurements and numerical tape modeling. The measurements are done at room temperature and in liquid nitrogen (LN_2) bath at atmospheric pressure.

The precise vertical linear motor stage (PVLS) shown in figure 1(a) is used as the warm part of the setup [6]. PVLS specifications for maximum force, travel and resolution are 20 kN, 200 mm and $0.05 \mu\text{m}$ respectively. The thrust bar can move up and down driven by the PVLS, which is placed on top of the stress–strain test rig. The force applied to the sample is measured with a 50 kg load cell. The tape is fixed between brass clamps with sanding paper (grid 150) that is glued to the clamps to prevent tape slipping. The sample

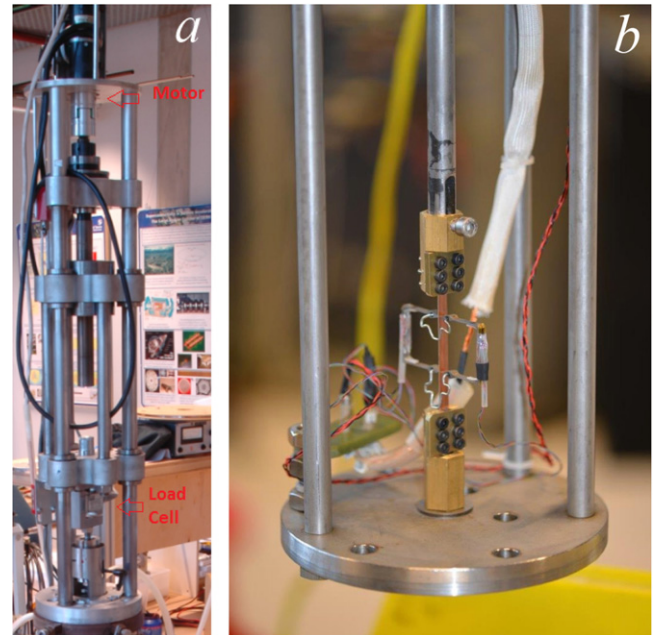


Figure 1. On the left (a) the precise vertical motor stage (PVLS) and on the right (b) a sample mounted in the setup with the clamps and double extensometer configuration.

length is 90 mm. The elongation of a tape sample is measured by a pair of extensometers. The extensometers are placed in the center of the sample and clamped with two springs as depicted in figure 1(b). The distance between the extensometer grips is 52 mm. The double extensometer configuration is used to compensate for bending effects. The signals from the extensometers are recorded separately and then averaged.

Before start of the measurement, the thrust bar is pulled towards the direction of the contact position until about 0.1 mm before the actual load is utilized. In this position no force is exerted on the tape sample. For liquid nitrogen measurements this distance is twice as much, anticipating the overall thermal compression of the setup during cooling down. The stress–strain test is started by pulling up the thrust bar. The displacement speed is set to $100 \mu\text{m s}^{-1}$, corresponding to a strain rate of $4 \times 10^{-4} \text{ s}^{-1}$. The tensile strain in the sample tape is defined as

$$\varepsilon = \Delta l / l_0 \quad (1)$$

with ε : strain, Δl : elongation and l_0 : initial length. With the initial cross-sectional area of the sample tape and the exerted tensile force on the sample, the tensile stress is

$$\sigma = F / A, \quad (2)$$

where F : force and A : initial cross-sectional area.

To assess the contribution of copper and Hasteloy layers to the stress–strain states of the tapes, two sets of samples were prepared. The first set consists of the SCS4050 tape samples without any modification to it. The second set are tapes with the copper layers etched by a FeCl_3 water solution. No other modification was applied to the second set of samples.

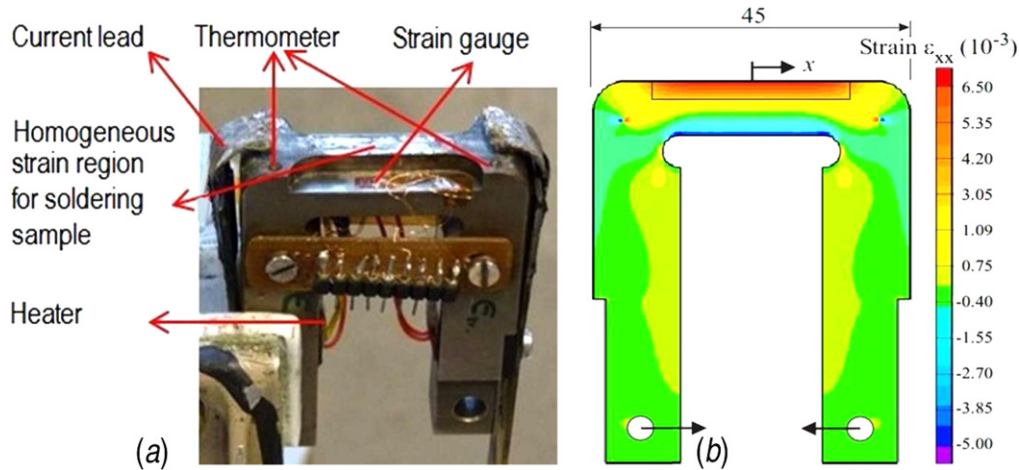


Figure 2. (a) The U-spring instrument; (b) FEM calculated strain profiles of the U-spring [7].

2.2. U-spring

The Ti-6Al-4V U-shaped bending spring (U-spring) [7], shown in figure 2, is used to measure the strain dependence of the tape critical current. The force is applied to the legs of the U-spring by an opposite-threaded rod and a worm-gear combination. Calibrated strain gauges are used to extrapolate to the applied axial strain in the central sample axis from the measured strains at the gauge positions next to the sample. Finite element method (FEM) calculations [7] of the U-spring mechanical behavior predict the strain to be homogeneous within 0.01% over a central region of 18 mm length, as shown in figure 2(b). The tape sample is soldered to the spring at the area with the homogeneous strain distribution. Soldering the tape to the U-spring allows applying compressive strain as well as tensile strain. The soldering takes place at a controlled temperature of 543 K. Cooling down the tape sample from 543 to 77 K causes a pre-strain in the ReBCO layer due to the difference in thermal contraction coefficients between U-spring material and HTS tape. We estimate the ReBCO layer pre-strain to be 0.01% at 77 K for a SCS4050 tape. The total length of the tape sample is 45 mm. Two pairs of voltage taps are attached on the tape surface at the center of the tested sample, with distances of 8 and 16 mm. The distance from the outer voltage tap to the current lead is 10 mm. The outer pair is used to check whether any entrance effect occurs.

The I_c is measured by the standard four-point probe method using a $10 \mu\text{V m}^{-1}$ criterion to determine the I_c value. For each applied strain, the $V-I$ curve is measured to determine the I_c and n -index. The n -index is calculated by fitting experimental $V-I$ data with the following equation

$$E = E_c \left(\frac{I}{I_c} \right)^n. \quad (3)$$

2.3. Torsion tensile strain setup

An experimental setup, which is able to apply torsional and tensile strains simultaneously, is specially developed to

investigate the effect of both combined loads. The setup is presented schematically in figure 3.

The PVLS motor stage described above is mounted on the top of the setup and allows stretching the sample in controlled increments. However, the PVLS motor stage displacement with $0.05 \mu\text{m}$ accuracy cannot be used as actual applied strain on the sample due to contraction and extension of different setup parts under load. The tensile load applied to the sample through the thrust bar is measured by a 50 kg load cell. The stress-strain relation for the tape has a nonlinear behavior associated with yielding of copper and hasteloy. That makes a calculation of the strain in the tape, simply by using the linear Young's modulus not correct due to change of the tape's modulus at higher stress level. Instead we use the measured strain-stress data from the purely tensile experiment (see figure 17) to get strain in the tape that corresponds to the stress measured in torsion-tensile setup. The tensile stress is calculated using relation (2) where F is the applied force measured by the load cell and A is the tape cross-section area calculated using SEM data on the tape thickness (see figure 10).

Torsion strain is applied by rotating the cylinder on the top of the setup. The cylinder is connected to the thrust bar and via the thrust bar to the sample. Pure torsional applied load measurements were done by changing the torsional angle, while the tensile load is set to zero. The angle increments were chosen 30° . After each measurement, the torsional angle was set back to zero value and the I_c and n -value reversibility was checked. The applied torsion is presented as a twist pitch

$$T_{\text{pitch}} = \frac{\theta}{L}, \quad (4)$$

where θ is rotation angle and L is the length of the specimen.

The pure tensile and combined torsion-tensile measurements were done at fixed torsional angle while tensile load was varied. After each increase of tensile load, the I_c and n -value reversibility was verified by removing the tensile load while the torsional angle remained unchanged. We used 50 N increments of the load for pure tensile test. For combined tests

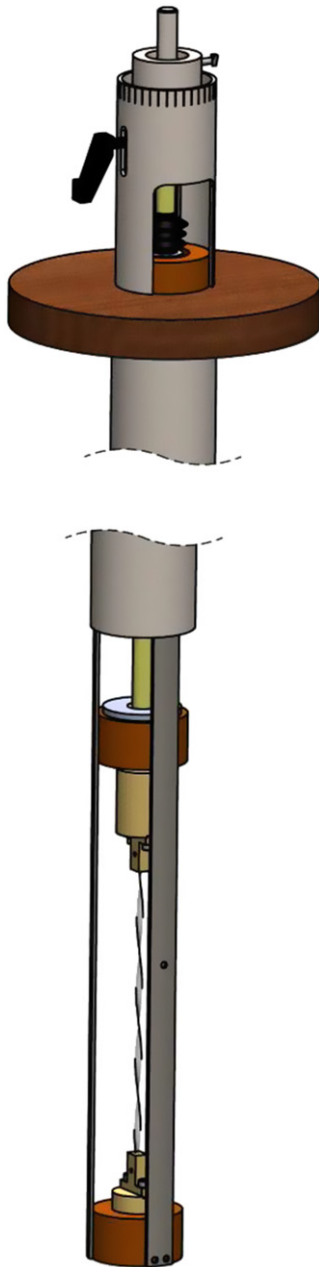


Figure 3. Sketch of torsion–tensile strain setup.

we used smaller 25 N tensile load steps while the torsional angle remained fixed.

The length of the tape samples used in the torsion–tensile tests is 170 mm. The sample ends are soldered to copper blocks, which also act as current leads. The V – I measurements are done using the four-probe method. After the sample is mounted in to the experimental setup, five voltage tap pairs are soldered along the sample length. The voltage tap pairs have 15 mm spacing and are located on the tape length axis, centered at the middle of the sample length to avoid boundary effects from the sample ends. Multiple voltage taps along the length are necessary to probe possible inhomogeneity of the samples' electro-mechanical properties. The I_c value presented below in the results section is an average value over five voltage taps. All soldering procedures are performed

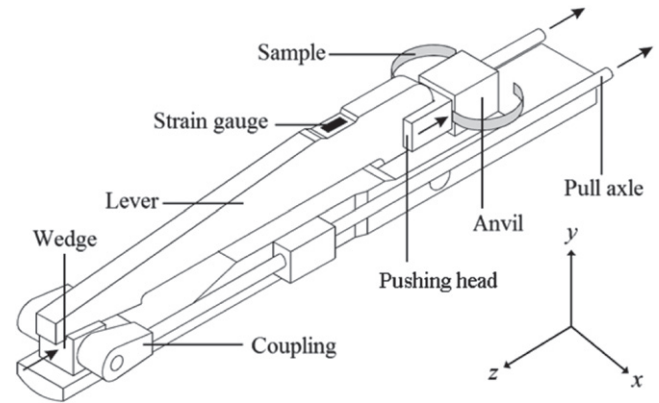


Figure 4. Schematic view of the transverse load setup.

taking into account minimum soldering temperature and heating time.

2.4. The transverse pressure setup

We use the press [8] shown at figure 4 to measure the I_c dependence of the tape versus applied transverse load.

The tape press applies a mechanical load to the flat side of a tape in transverse direction in a LN_2 bath. The applied force is controlled outside the cryostat on a continuous scale. On the top of the lever, an interchangeable pushing head is mounted. After a sample mounted, the pushing head is pre-loaded by small springs resulting in a self-adjustment of the pushing head plane-parallel to the sample surface. The force applied to the pushing head is measured by the calibrated strain gauge attached to the lever. To establish the relation between applied force and strain gauge voltage a calibration measurement was performed in LN_2 bath. The calibration procedure is as follows. One side of the lever is pulled by a stainless still wire while the pulling force is measured by a 50 kg load cell. Twenty data points are taken to determine the linear relation between strain gauge voltage and the force applied to the lever. The force applied to the pushing head is increased by the lever mechanism with a ratio 1:10 compared with the force measured by the load cell. When we take into account the load cell error, the lever length tolerance and the strain gauge voltage reading uncertainty, the estimated error bar of the measured force is then ± 60 N.

The experiments are carried out in LN_2 under atmospheric pressure conditions and it must be taken into account that the I_c changes significantly with temperature variations induced by atmospheric pressure fluctuations. In order to compensate for temperature variations due to changing environment pressure, a Cernox CX-1050-SD-HT-1.4L type resistive thermometer (with temperature uncertainty ± 16 mK) is used to monitor the actual temperature of the tape during measurement. The thermometer is attached to the anvil surface close to the pushing area. All the I_c data are corrected to a temperature of 77.36 K. Literature data [9] on the critical current versus temperature dependence of SCS4050 tape was used for this correction. A 150 mm length of sample tape is used for the tests. The voltage taps are soldered to the tape

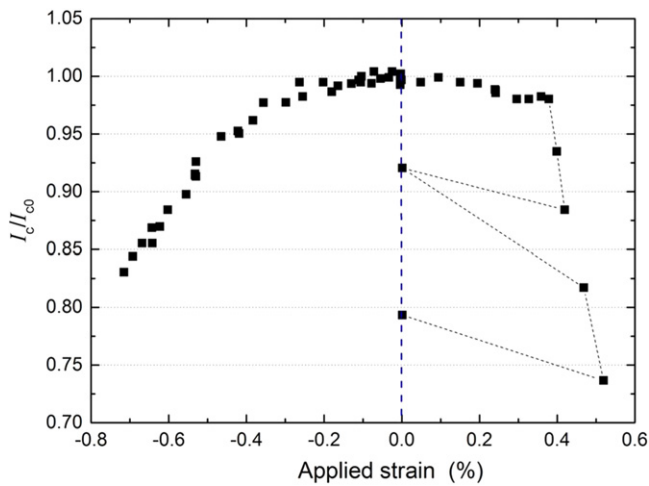


Figure 5. Normalized critical current as a function of applied axial strain in ReBCO layer at 77 K and in self-field.

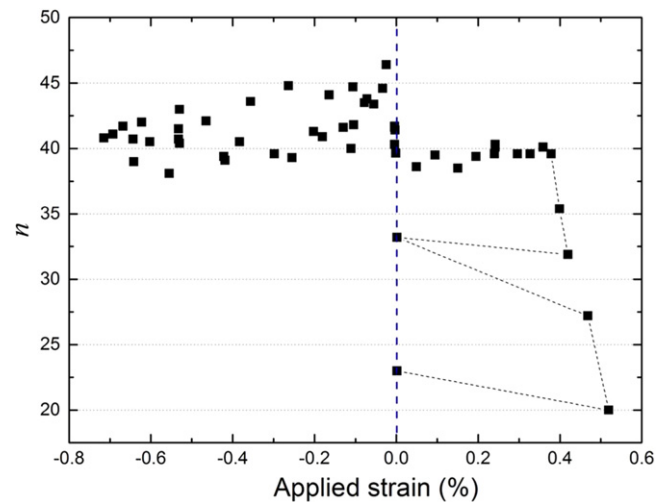


Figure 6. The n value as a function of applied axial strain in ReBCO layer.

surface in the middle with a distance of 10 mm between them. The temperature did not exceed 350 °C during soldering of the voltage taps as well as during soldering the tape to the current leads; the soldering time was less than 30 s; non-aggressive soldering flux was used. All samples were measured using the tape orientation with ReBCO side to the anvil.

Different measurement procedures are defined, changing e.g. cycling sequences, but for every test the I_{c0} and n -index of the virgin (unloaded) sample is determined first. Most samples are tested such that after a transverse load is applied, the I_c and n -index are measured in loaded state. If no I_c degradation is observed, the load is increased further and the measurement is repeated. In case an I_c degradation is observed, the load is released to zero and the I_c reversibility is checked. Also several samples were tested with ‘cycling load’. For each selected load level we cycled 10 times between zero and the chosen load before performing a V – I measurement. After cycling, the I_c and n -index were determined in loaded state and if no I_c and n -value degradation is observed, the load level is increased further and cycling of the load is repeated. In case of an observed I_c degradation, the load-unload cycles are repeated at the same load level, with a V – I measurement at the end of a cycle without load, until the I_c degradation saturates.

3. Measurements results

3.1. Axial strain

Figures 5 and 6 show the results of I_c/I_{c0} and n values versus applied axial strain obtained using the U-spring setup at 77 K and self-field. The measurements showed the irreversible intrinsic strain limit in the ReBCO layer to be $\sim 0.40\%$. Taking into account the estimated pre-strain in the ReBCO layer gives an intrinsic strain value of $\sim 0.41\%$, which is in good agreement with literature data [5]. The degradation cliff is clearly indicated on the I_c/I_{c0} and n value curves versus applied strain (figures 5 and 6). We took the virgin sample I_c

(i.e. no applied strain) as I_{c0} for the normalized plots showing the results. As in many reports, often an I_c criterion of $100 \mu\text{V m}^{-1}$ is used for HTS conductors; we prefer to present the data using an I_c criterion of $10 \mu\text{V m}^{-1}$, a more suitable criterion in view of superconducting coil design. At the same time this explains why our data show a bit more scatter due to the noise level linked with the short test sample length.

It is clear that for cable applications the strain in the ReBCO layer should remain sufficiently below the irreversibility limit but at the same time severe compressive strain results into loss of current density.

3.2. Tension and torsion

We used four samples with different combinations of combined axial tensile and torsional load for measurements. Also here an electric field criterion of $10 \mu\text{V m}^{-1}$ is used for the I_c measurements, all data taken at 77 K and in self-field with use of torsion tensile experimental setup. One sample (1) is exclusively subjected to tensile axial load and no torsion. Torsional angles for two other samples (2 and 3 respectively) are 300° and 480° , corresponding to 1.8 and 2.8 grad mm^{-1} twist pitch respectively. Finally a pure torsional measurement is performed on sample 4, eventually up to 990° resulting into 5.8 grad mm^{-1} maximum twist pitch.

3.2.1. Pure tensile strain and combined torsion–tensile tests.

Figure 7 shows I_c/I_{c0} as a function of tensile strain for three samples. The sample measured under pure tensile load showed 95% of I_{c0} at tensile strain $\varepsilon_{\text{tens}} \sim 0.55\%$. The measured value is higher than $\varepsilon_{\text{tens}} \sim 0.45\%$ given by the manufacturer for 95% of I_c [4]. The higher value is explained by our method of taking into account the nonlinear behavior of the stress–strain dependence and lower (actual) cross-sectional area ($3.472 \times 10^{-7} \text{ m}^2$) of the tape determined from SEM pictures (see chapter 3.3). At the same time we have a perfect agreement with manufacturer data with $\varepsilon_{\text{tens}} \sim 0.45\%$ strain for 95% of I_c while taking the Young’s modulus

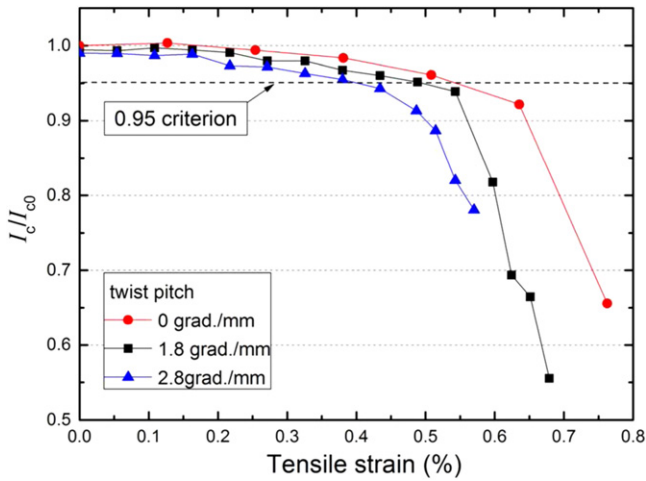


Figure 7. The I_c/I_{c0} versus applied axial tensile strain for different torsion angles on SCS4050 tape.

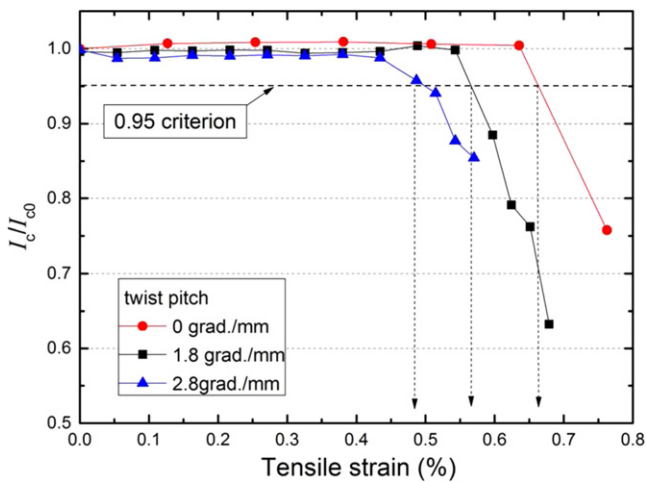


Figure 8. The I_c reversibility behavior for data points taken at zero tensile load. The tensile strain scale represents the maximum strain level reached before the reversibility check.

$E = 116.7$ GPa [10] and tape cross-sectional area 4×10^{-7} m² [4]. Up to $\varepsilon_{\text{tens}} \sim 0.63\%$, the I_c reversibility is found to be about 100%, as illustrated in figure 8. The criterion we use to define the critical tensile strain is the applied strain after which the critical current becomes lower than 95% of I_{c0} when tensile load is removed (figure 8). The irreversible degradation starts at loads higher than $\varepsilon_{\text{tens}} \sim 0.63\%$ for pure tensile load. The n -index, a very sensitive indicator for ReBCO layer damage, stayed constant up to $\varepsilon_{\text{tens}} \sim 0.63\%$, after which it dropped sharply.

The I_c decrease for combined torsion–tensile measurements started earlier compared with pure tensile load. For the sample with 1.8 grad mm^{-1} twist pitch the irreversible I_c degradation was observed at $\varepsilon_{\text{tens}} \sim 0.56\%$. When the twist pitch is increased to 2.8 grad mm^{-1} , the irreversibility limit decreases to $\sim 0.48\%$ applied strain, see figure 8. Majkic *et al* [11] found similar behavior of a ReBCO tape under combined torsion–tensile stress.

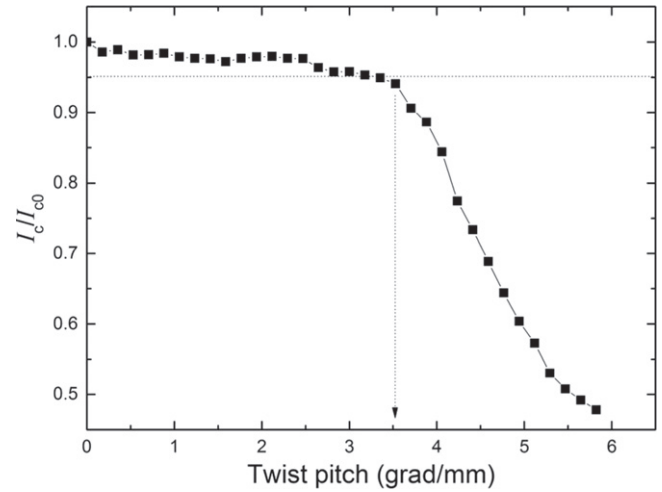


Figure 9. Normalized critical current as a function of the twist pitch.

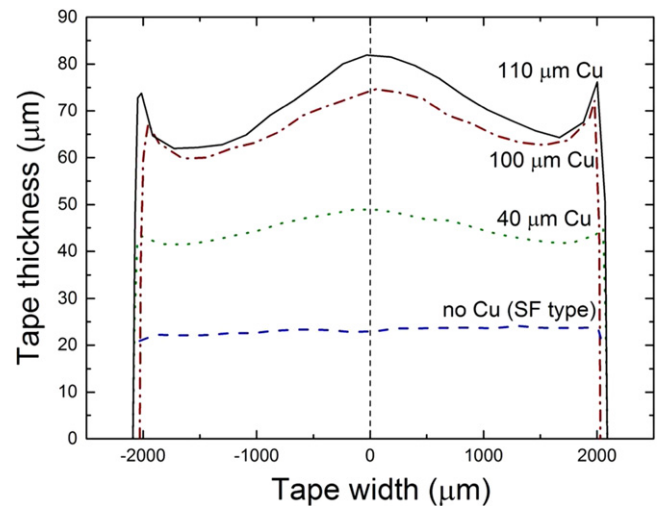


Figure 10. Average thickness profiles of different types of SuperPower[®] tapes, each taken from ten cross section samples.

3.2.2. Pure torsional strain test. The tape under pure torsion shows only $\sim 2\%$ I_c degradation up to 2.5 grad mm^{-1} twist pitch. After 3.5 grad mm^{-1} twist pitch the I_c starts to decrease fast and the I_c degradation becomes irreversible (figure 9). The twist pitch homogeneity was verified after the final measurement. We found up to 13% of length variations between 180° twist steps. To minimize the influence of twist pitch inhomogeneity, the average value of I_c from the five voltage taps along the sample length is presented.

The measurement conditions and results for the four tested axial tensile–torsion samples are summarized in table 1.

3.3. Transverse loading

We used SCS4050 tapes with $40 \mu\text{m}$ (standard tape), 100 and $110 \mu\text{m}$ total thickness of copper layers (we count the total thickness of the copper on both sides of the tape) to study the influence of transverse load on the I_c degradation in relation to the copper layer thickness. A SF4050 type tape without copper layer was also included in measurement sequence.

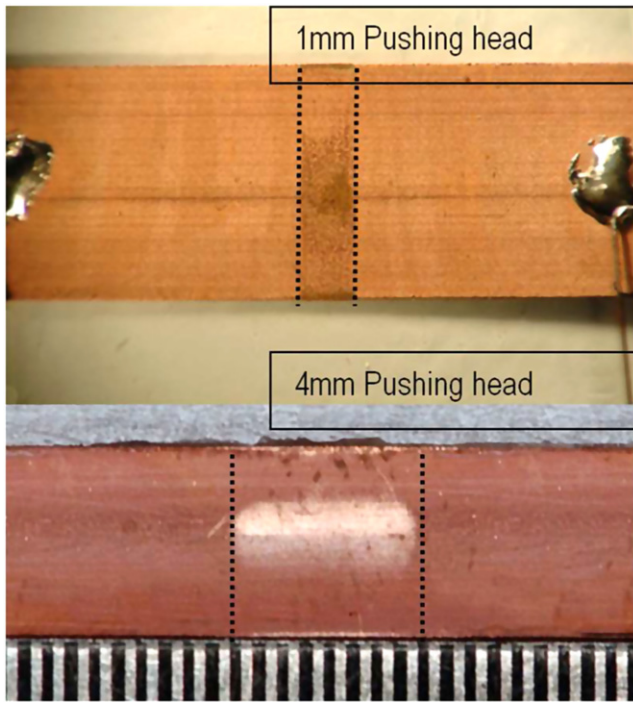


Figure 11. Pushing head footprint marks on SCS4050 tapes with $40\ \mu\text{m}$ (standard tape) after transverse loading with 1 and 4 mm width pushing heads. The dashed lines indicate the pushing head areas.

The cross section thickness profile of the tapes along their width was measured prior to the transverse load measurements. We used ten slices of each tape to measure the thickness profile of the tapes. Figure 10 presents the average values of the tape thickness profile measured from the tape centre line and averaged over ten measured slices. The measurements showed that the SCS4050 tape with $110\ \mu\text{m}$ copper layer has the largest thickness variation while the SF4050 tape without copper has almost uniform thickness along its width. This indicates that the copper layer is responsible for the thickness variation, which increases with the layer thickness. The effect, referred to as ‘dog boning’, is attributed to the copper electroplating process, creating the inhomogeneous layer thickness.

The variation of the tape thickness has a significant effect on the actual contact area between tape and pushing head in the transverse load press. Figure 11 shows the footprint marks from a 4 and 1 mm pushing head on a standard $40\ \mu\text{m}$ Cu layer tape. It is clear from the footprint profile that contact area is not uniform over the tape width and the main contact area is concentrated in the center of the tape.

Regardless to the actual contact area variation, the pressure is calculated as the applied force divided by the area taken as pushing head width multiplied by tape width. Data for all samples measured with the 1 mm width pushing head are gathered in figure 12. Both, the force and assumed average pressure are given, since the applied force is measured directly while the actual contact area is not well defined.

A clear correlation is observed between the copper thickness and the applied force level where I_c degradation first

occurs. The level of critical force is reduced with increasing copper layer thickness. The force applied to the SF4050 tape (without Cu layer) was up to 3.5 kN (the upper limit of the used press), but no clear I_c degradation could be observed. Tapes with 40, 100 and $110\ \mu\text{m}$ copper layers have 3.02, 1.61 and 1.29 kN critical forces respectively. That indicates the strong influence of the Cu layer thickness on tape performance upon transverse loading. Arriving at this point, it is not exclusively clear whether the influence of the Cu thickness on the critical transverse force is due to plasticity, creating tensile strain in tape plane direction, or if the Cu layer thickness inhomogeneity is dominant compared to the absolute layer thickness. This problem will be further investigated.

Two tapes with 40 and $110\ \mu\text{m}$ Cu layer were subjected to cycling transverse load ten times between each set load level and zero, subsequently increasing the load level, to study the influence of cycling on the I_c degradation. Figure 13 shows the I_c/I_{c0} data for tapes measured with and without cycling of the load. The tape with $40\ \mu\text{m}$ Cu layer was measured using 2 mm width pushing head while $110\ \mu\text{m}$ Cu layer tape was measured with 1 mm width pushing head. We plot I_c/I_{c0} against pressure in figure 13 in order to compare samples measured with different pushing heads. Figure 13 shows that samples measured with cycling load showed earlier and faster degradation compared with tapes measured without cycling load, though the difference in critical pressure is small.

4. Modeling

We model numerically the stress–strain state of the tape originating from the tape production process and three cases of load: (1) tensile (2) combination of tensile and torsion and (3) transverse load at 77 K. The relevant loading experiments at 77 K described above serve as a validation for the outcome of the model, while separate experiments are performed to acquire the crucial specific thermo-mechanical properties of the dominant layers, the Hastelloy substrate and electroplated copper.

The main goal of the modeling is to calculate the strain state in the ReBCO layer. As it is shown in [5], the residual strain in the ReBCO layer after the production process is significant compared with the critical strain (see figure 14) and therefore we have to take it into account.

Figure 15 shows the configuration of SuperPower[®] 2G HTS tape SCS4050. In our model we exclude the buffer and silver layers because these layers have no relevant influence on the mechanical behavior due to their small thickness [5]. Thus we keep only three materials in the model: substrate (Hastelloy C-276), copper and ReBCO. The ReBCO layer has also small thickness ($\sim 1\ \mu\text{m}$) but this layer is needed to calculate the strain in it (see introduction and formula (6)).

We simulate the temperature variation during the production process to obtain the residual strain in the ReBCO layer. The sequence of the simulation steps for each load case is shown schematically in figure 16.

Table 1. Conditions and degradation levels for torsion–tensile measurements.

Sample #	Type of measurement	Max. ϵ_{tens} %	Max. torsion grad mm^{-1}	Degradation level	
				ϵ_{tens} %	grad mm^{-1}
1	Pure tensile	0.76	0.00	0.67	0.00
2	Combined	0.67	1.80	0.56	1.80
3	Combined	0.57	2.80	0.48	2.80
4	Pure torsion	0.00	5.80	0.00	3.50

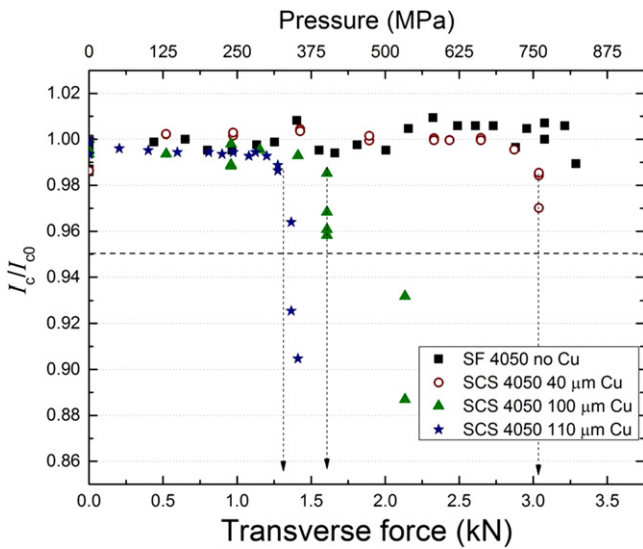


Figure 12. I_c/I_{c0} as a function of applied force (and average pressure) for tapes with different Cu layer thickness.

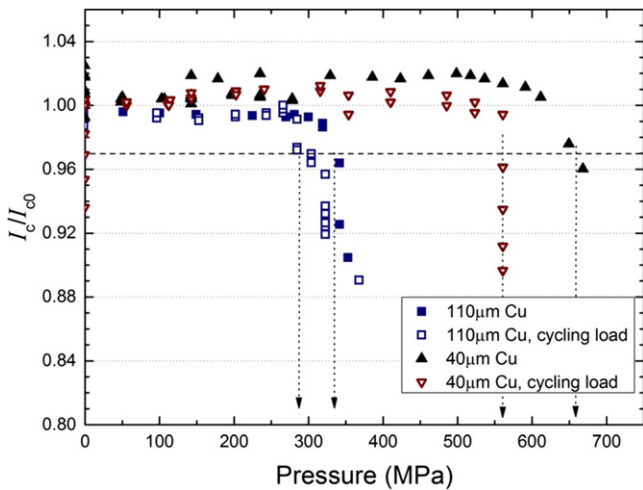


Figure 13. I_c/I_{c0} as a function of the applied average pressure with and without load cycling for tapes with 110 and 40 μm Cu layer thickness.

We divide the modeling of the tape production into two main stages: the first one is the metal organic chemical vapour deposition (MOCVD) process that creates the ReBCO film on the substrate and the second step is the copper electroplating to create the copper stabilizing layers. The MOCVD process takes place at a temperature of about 1020 K, then it drops to 350 K for the copper electroplating, and finally it decreases to

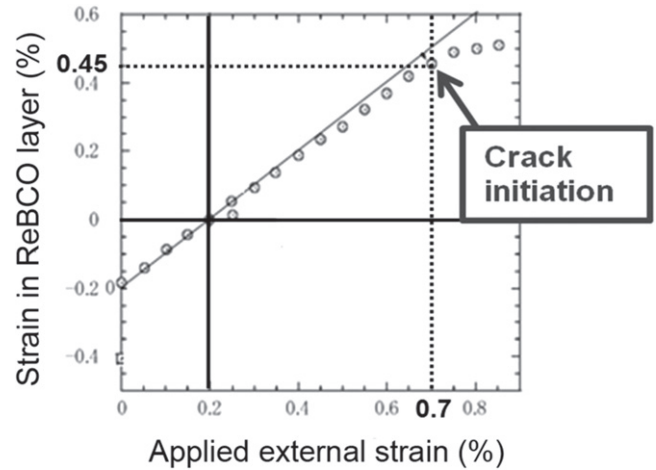


Figure 14. State of strain on the YBCO layer as a function of applied external tensile strain at room temperature (RT), (courtesy of Osamura *et al* [5]).

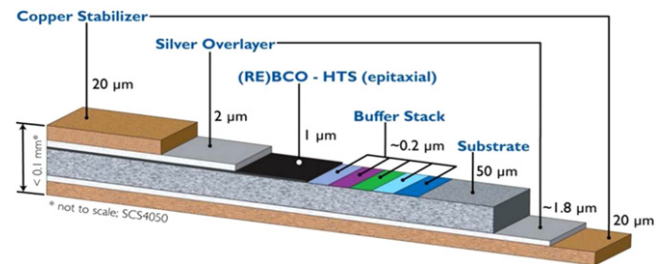


Figure 15. Configuration of SuperPower[®] 2G HTS Tape SCS4050 [4].

room temperature and eventually to 77 K at operating or testing conditions (figure 16). We are aware of the oxygenation process of the ReBCO layer that takes place during the tape production and goes accompanied with lattice distortion, but do not include this into the model. This step is excluded first of all due to lack of required processing parameters of the oxygenation step for the tape in subject.

4.1. Properties of materials

Since for the model we account for a wide range of temperatures (77–1020 K) and plastic behavior of the materials, we need to know the thermal expansion coefficients, the elasto-plastic material properties and their dependence on temperature. We assume that all materials of the tape are isotropic and the behavior of ReBCO in the whole temperature range is elastic (table 2). Later on we will find that this

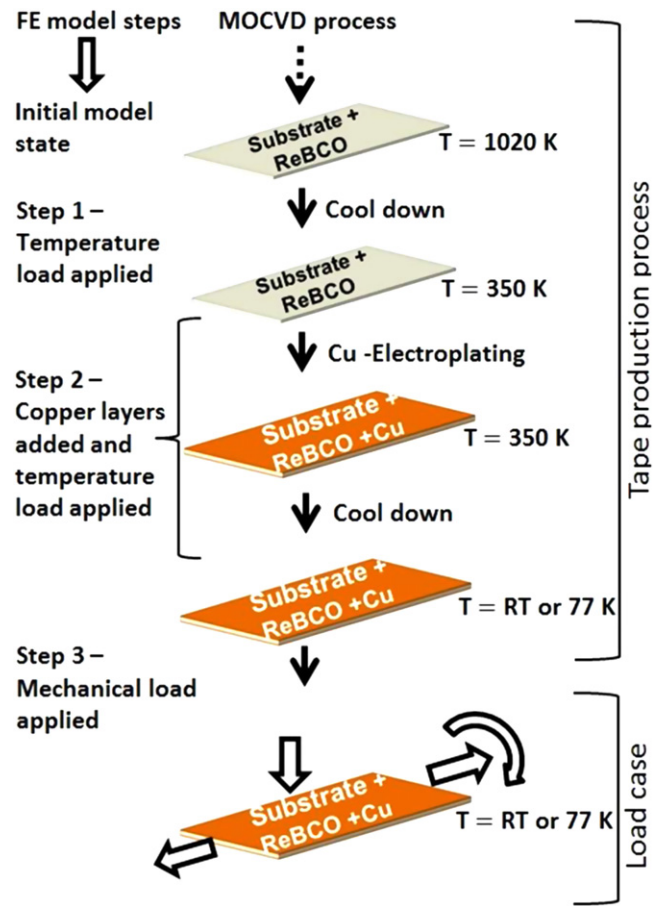


Figure 16. Modeling steps for the production process of the ReBCO composite tape.

Table 2. Elastic properties of ReBCO.

Young's modulus (GPa)	157 [12]
Poisson ratio	0.3 [12]
Thermal expansion coefficient (K ⁻¹)	1.1·10 ⁻⁵ [5]

assumption is justified by the comparison between FE model and experimental results.

The stress–strain dependence for SCS4050 tape and Hastelloy (the tape without copper) and copper at 77 K and RT was obtained from tensile stress–strain loading experiments (see section 2.3 for the method description). Figure 17 shows the experimental results of the stress–strain dependence for the SCS4050 tape and Hastelloy, the calculated stress–strain dependence of copper is also shown.

It seems to get the properties of thin copper layer experimentally is quite difficult. Therefore we calculate it using the mixture rule (5) and experimental data for the hastelloy and the tape. It should be noted that the mixture rule is applicable not only for the elastic constants of a composite structure, but also for the elasto-plastic properties [13].

$$\sigma_{\text{Tape}}(\epsilon) = \sum V_i \sigma_i(\epsilon) \approx V_{\text{Hast}} \sigma_{\text{Hast}}(\epsilon) + V_{\text{Cu}} \sigma_{\text{Cu}}(\epsilon), \quad (5)$$

where the subscripts 'i' indicate the tape materials; $\sigma_{\text{Tape}}(\epsilon)$, $\sigma_{\text{Hast}}(\epsilon)$ and $\sigma_{\text{Cu}}(\epsilon)$ are the stress (σ)–strain (ϵ) dependence

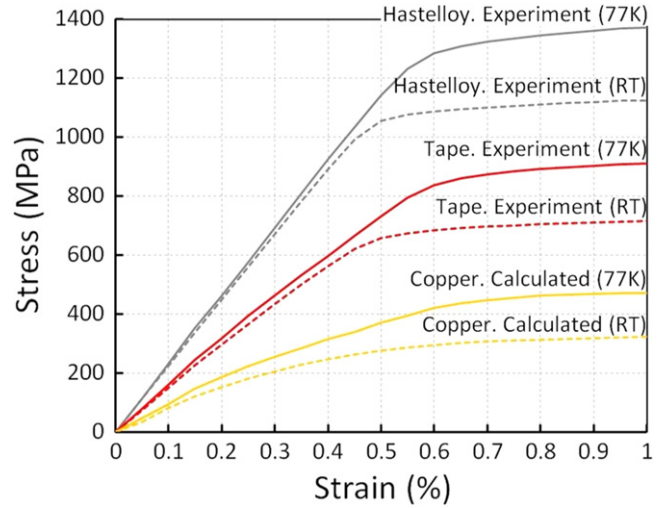


Figure 17. The stress–strain curves at RT and 77 K for the SCS4050 tape, Hastelloy and copper.

for the whole tape, hastelloy and copper respectively; V_i is the volume fraction of component i.

In our samples the average values of the volume fractions are $V_{\text{Hast}} = 52.7\%$, $V_{\text{Cu}} = 47.3\%$. These values were obtained from microscopic observations on a few samples cross-sections.

The elastic properties, yield stress and thermal expansion coefficient are presented in table 3. The Young's modulus and yield stress are obtained from the initial linear part of the stress–strain curves (figure 17).

We also input the plastic properties of the Hastelloy and copper as digitized data of nonlinear parts of the stress–strain curves in the FE model (figure 17).

We assume RT elasto-plastic properties of Hastelloy and copper at the temperatures above RT and in the range between RT and 77 K we assume linear dependence of the properties with temperature. The thermal expansion coefficients are assumed constant at any temperature. Properties of the ReBCO are also taken independent on temperature.

4.2. Tensile test simulation

In this section we present the FE model for the purely axial tensile load case. This modeling has two aims:

- (1) to validate the material properties.
- (2) To validate the criterion of the initial critical current degradation.

The geometry and finite element mesh are shown in figure 18. It is a piece of tape of 4 mm width by 5 mm length. As we consider tensile load only, the model has two planes of symmetry. Therefore we use only one quarter of the sample with symmetric boundary conditions (BC) on two sides to reduce the calculation time. For the mesh of this model we use the 8-nodes reduced integration brick finite element C3D8R⁴. For better approximation through the thickness, we

⁴ ABAQUS™ documentation.

Table 3. Elasto-plastic properties and thermal expansion coefficient of Hastelloy and copper.

	Young's modulus (GPa)	Yield stress (MPa)	Poisson ratio	Thermal expansion coefficient (K^{-1})
Hastelloy (RT)	223	891	0.307 [14]	1.34×10^{-5} [5]
Hastelloy (77 K)	228	1141	0.307 [14]	1.34×10^{-5} [5]
Copper (RT)	80	120	0.34 [16]	1.77×10^{-5} [5]
Copper (77 K)	98	146	0.34 [16]	1.77×10^{-5} [5]

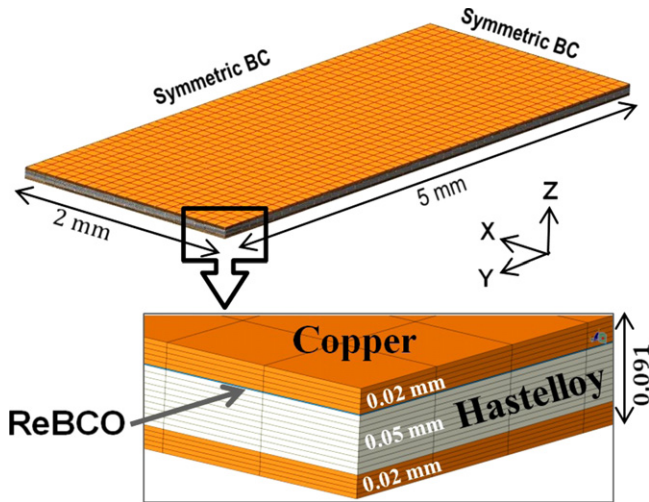


Figure 18. The geometry, FE mesh and boundary conditions (BC) for the axial tensile test simulation.

use five elements for each copper layer, ten elements for the Hastelloy and one element for the ReBCO layer. We verified the effect of selecting just one element for the REBCO layer by choosing more elements but the effect on the result was negligible. Thus the size of one element is approximately $0.1 \times 0.1 \times 0.004$ mm for the Hastelloy and the copper, and $0.1 \times 0.1 \times 0.001$ mm for the ReBCO.

In accordance with the production process we have three steps in the FE model (figure 16). First we consider a $\Delta T = 670$ K cooling step. Second we add copper layers and model the stress–strain state due to a $\Delta T = 60$ or 236 K cooling steps (cooling to RT or 77 K respectively). In the third step we apply the tensile load as a displacement boundary condition along the Y-axis by 1% tape deformation (0.05 mm) on the nodes of one short side of the tape. To the other end of the tape we apply fixed boundary condition (nodes displacement along Y axes equals 0). The results of the tensile test modeling at RT and 77 K are presented in figure 19 in terms of stress–strain dependence for the tape. The experimental and modeling results are in excellent agreement. Probably the small difference may be due to the fact that we do not account for the buffer and silver layers in our model.

Figure 20 shows the dependence of the strain in the ReBCO layer at 77 K on the applied external strain obtained from the FEM calculation. It can be seen that the value of ReBCO strain for a free standing tape, that is after the production process and cool down to 77 K with zero applied external strain, is $\epsilon_{ReBCO} = -0.237\%$. This curve is linear

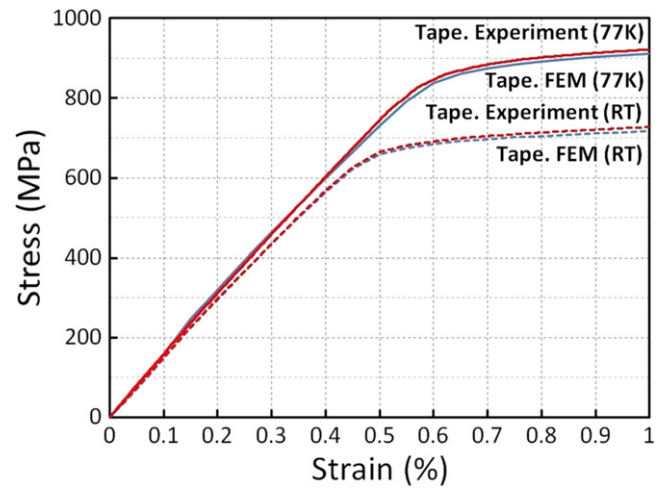


Figure 19. Comparison of the tensile experiments with modeling results for the tape at RT and 77 K.

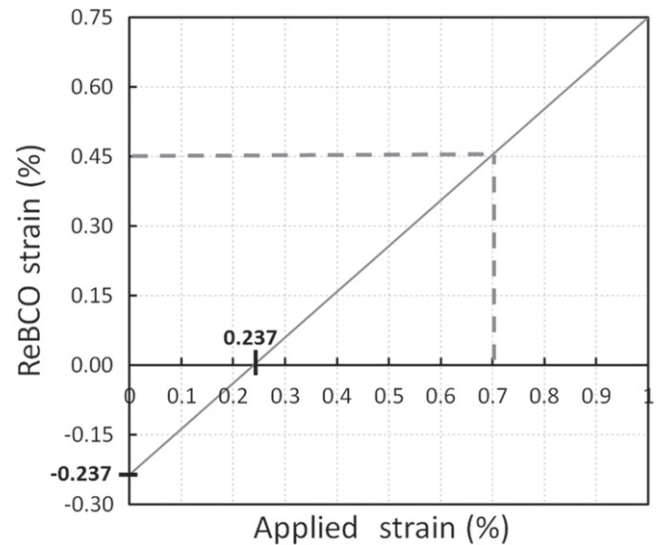


Figure 20. FEM calculation of strain on the ReBCO layer as a function of applied external tensile strain at 77 K.

and the slope of this curve is 45° . This is because we assume fully elastic ReBCO material properties in the FE model, thus $\epsilon_{ReBCO} = \epsilon_{External} + \epsilon_{Residual ReBCO}$, where $\epsilon_{External}$ is the external applied strain and $\epsilon_{Residual ReBCO}$ is the residual strain in the ReBCO layer after the production process and cool down to 77 K.

The residual strain in the ReBCO layer at RT and 77 K, which is calculated analytically, obtained experimentally [5] and by our FE modeling of the production process is

Table 4. Residual strain in the ReBCO layer of SCS4050 tape at RT and 77 K.

	ϵ_{ReBCO} (%), RT	ϵ_{ReBCO} (%), 77 K
Analytical [5]	-0.17	-0.26
Experiment [5]	-0.20	—
FEM	-0.17	-0.24

presented in table 4. It can be seen that our results are similar to the analytical and experimental results from [5].

Figure 21 shows the critical stress and strain obtained from FEM calculation and experimentally. In each curve we indicate the points corresponding to the critical current degradation. For the FEM calculation this point corresponds to the strain of the ReBCO layer $\epsilon_{ReBCO} = 0.45\%$ (critical strain of ReBCO layer). For the experimental curve this point corresponds to the irreversible degradation of critical current (section 3). The values of critical stress and strain are presented in table 5.

The values of critical stress and strain from FEM and experiment are very close to each other. Thus, we can conclude that:

- (1) using the properties obtained experimentally and the mixture rule, and comparing the simulation and experimental results we conclude that our model adequately describes the experiment.
- (2) Assuming that 0.45% critical strain of the ReBCO layer leads to the beginning of degradation of critical current, we find the corresponding critical strain in the whole tape (0.70%) (figure 20). This critical strain is very close to one obtained experimentally (0.67%, figure 21). This means that the 0.45% criterion is the appropriate criterion for these type of models.

4.3. Simulation of torsional–tensile load combination

In this section we present the FE model for the combination of tensile and torsional load and compare the simulations with the experimental results. The corresponding experiment is presented in section 3. This modeling aims at validation of the irreversibility strain criterion (0.45% strain in ReBCO layer) marked by the start of critical current degradation under tensile and torsional load combinations. In this model we use the same material properties, the same structure of the layers and the same first steps for modeling of production process as for the previously described axial tensile stress model. The main difference between these models is the other type of load. We apply the tensile and then torsion load to the tape instead of only tensile load.

In our FE model we created a tape section of $4 \times 80 \times 0.091$ mm (see figure 22) whereas the length of the tape is 80 mm. The 5 mm pieces at the tape ends are reserved for the clamps. The length of 70 mm between the clamps is chosen in order to avoid the influence of the edge effect of the clamps on the strain in the middle of the tape. Another

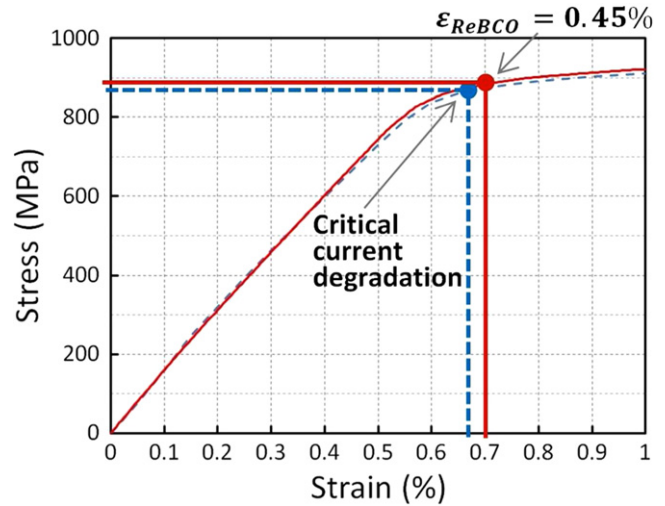


Figure 21. Critical stress and strain for the tape under tensile load at 77 K.

Table 5. Critical stress and strain of SCS4050 tape under tensile load at 77 K.

	Critical stress (MPa)	Critical strain (%)
Experiment (section 3)	864	0.67
FEM	883	0.70

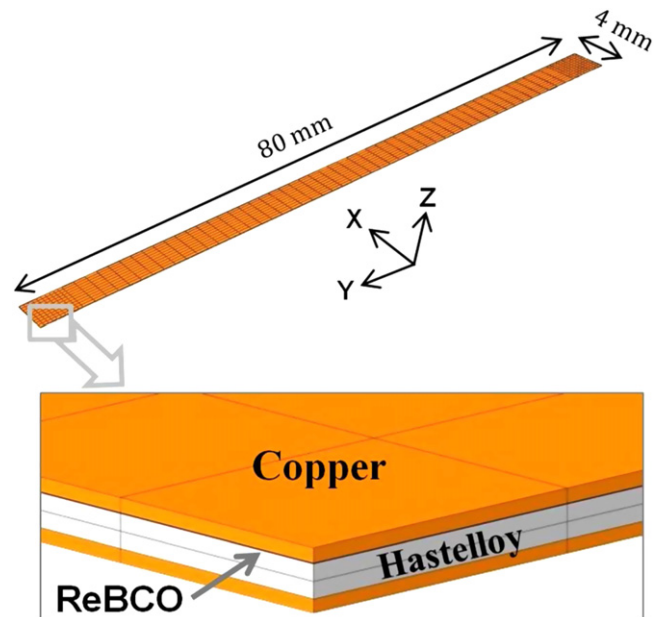


Figure 22. The geometry and FE mesh for the combination of tensile and torsional modeling.

consideration is to get a reasonable balance between the FE mesh size and calculation time.

We use C3D20 brick finite element instead of the C3D8R used for the pure tensile model. The element has 20-nodes and a full integration second-order element. Software developers of ABAQUS recommend using this type of element to model torsion and bending loads of composite materials and

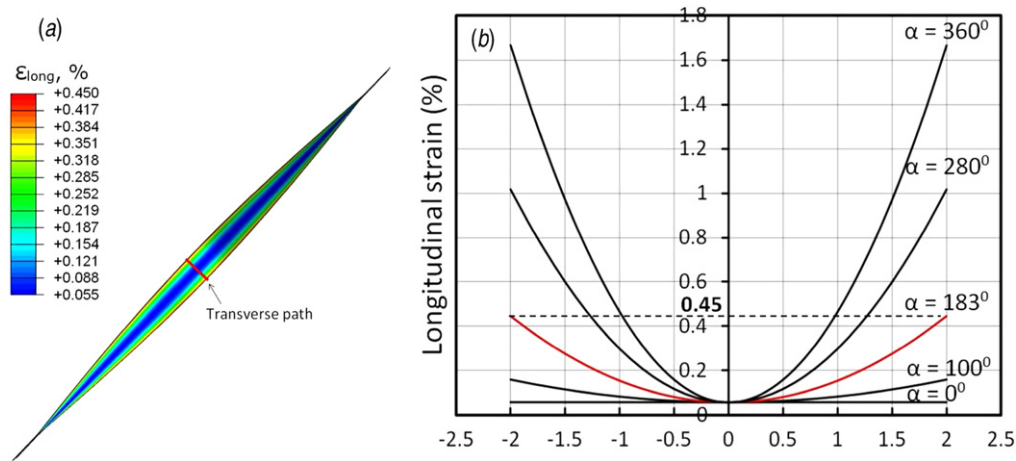


Figure 23. The distribution of longitudinal strain in the ReBCO layer for the combination of 0.3% applied tensile strain and a rotation angle of 183° (a). The longitudinal strain in the ReBCO layer along the transverse path for the combination of 0.3% applied tensile strain and different rotation angles (b).

defining only one element through the thickness of one layer (see footnote 4). We use one element for the thickness of the copper and ReBCO layers and two for the Hastelloy layer, 10 elements in width and 70 in length direction (see figure 22).

The sequence of the FE model steps is taken as following (see table 6). In the first two steps we model the production process of the tape (similarly to the tensile model). In the third step the ends of the tape are fixed by clamps. For this we create four absolutely rigid boxes ($5 \times 5 \times 1$ mm) in our model and apply displacement BCs to them. For the contact condition between the clamps and the tape, we assign the friction coefficient equal to 1 in order to avoid slip. In the next step we apply the tensile displacement boundary condition along the tape axis to one pair of the clamps at one tape end and a fixed boundary condition to the pair of the clamps at the other tape end. In the last step we add the rotation boundary condition to one pair of clamps.

As one of the results, the distribution of longitudinal strain in the ReBCO layer under the combination of applied tensile load (0.3%) and torsional load (rotation angle equal 183°) is shown in figure 23(a). Figure 23(b) shows the longitudinal strain along the transverse path of the ReBCO layer for different rotation angles. We present the longitudinal strain because the strain components in the other directions are lower.

The maximum strain is found at the edge of the ReBCO layer and for a fixed axial tensile strain on the tape of 0.3%, it reaches the critical value of 0.45% at 183° rotation load.

We calculate 20 variants of the tensile load from 0 to 1% with a step size of 0.05%. After each tensile load, we apply torsion from zero to 360° . For each tensile load, we find the torsion angle (α_{crit}) at which the longitudinal strain in the ReBCO layer reaches 0.45%. Following this criterion, we assume that at specified tensile load and the angle of the rotation greater than α_{crit} the critical current begins to degrade. Figure 24 shows the dependence of the critical strain in the ReBCO layer on applied external tensile and torsional strain for both, the FE model and the experimental results. The

points located below the curves indicate that the critical current does not degrade irreversibly for this combination of tensile and torsional loads. On the other hand the area above the curves represents permanent degradation region. There is a quite good but not ideal correlation between the FEM and the experimental results, deviating more for increasing torsional strain. The most likely explanation for this difference is that the sensitivity for detecting irreversibility is sufficiently high for pure tensile strain, but very small for torsional strain at an I_c -criterion of $10 \mu\text{V m}^{-1}$ since the ReBCO damage is only at the outer edge of the tape. This small amount of ReBCO irreversible degradation only gives a very small voltage rise and so the I_c criterion is reached only after larger applied torsion. Actually, the model should take into account an amount of ReBCO damage that is representative for an electric field level similar to that experienced at the purely axial tensile load. Altogether, the comparison is quite satisfactory.

Thus we can conclude that the FE model for combination of tensile and torsion load and the criterion 0.45% critical strain of the ReBCO layer for determination of critical tensile and torsion strain for the whole tape is valid.




4.4. Simulation of transverse load

This section is dedicated to modeling of compressive transverse load applied to the tape. The aim of this modeling is to understand the damage mechanism of the ReBCO layer under this type of load and to check whether the criterion of 0.45% strain in the ReBCO layer is valid as a starting point for irreversible critical current degradation.

We model transverse load on the tapes with 40, 100 and $110 \mu\text{m}$ thickness of the copper layer (see chapter 3.3) and without copper.

As our study demonstrates, the main difficulty of this case is that the tape surface is not flat; it has a non-uniform profile over the width of the tape. The difference between the maximum and minimum thickness of the tape cross-section is up to $15 \mu\text{m}$. The tape has a maximum thickness in the middle

Table 6. The sequence of the FE model steps for tensile and torsional load combination.

Step	Deformation of the tape at the end of a step	Type of load
3		Clamps attached to the tape ends at RT and cooling to 77 K.
4		Tensile load applied.
5		Torsion load applied.

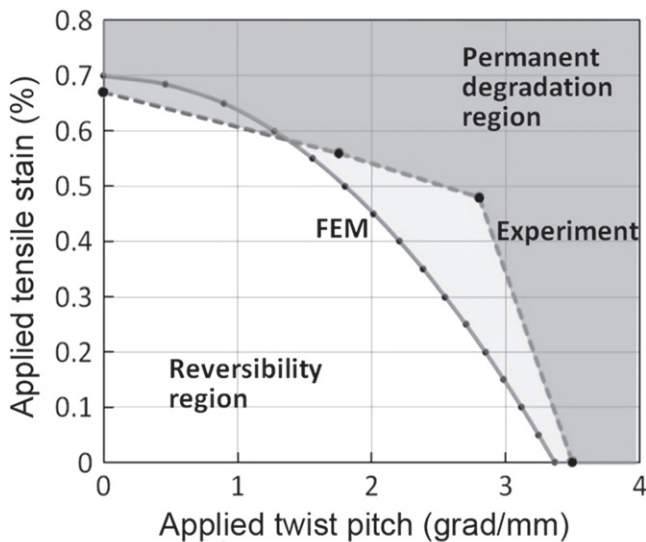


Figure 24. Critical strain in ReBCO layer as a function of applied external strain and applied torsion at 77 K from FE model and experimental results.

of the tape cross-section, then it decreases to a minimum value towards the edges, with an increase again near the tape edges (figure 10). This irregular shape is due to the copper electroplating process. The thickness of the hastelloy is observed to be quite uniform.

Such non-flat profile of the tape has no noteworthy effect on the critical load under tensile or combination of tensile and torsional load because these loads are applied in the longitudinal direction.

We cannot compare the critical pressure obtained from the experiment and FEM calculation because we do not know the real contact area between the pushing head and the tape surface. Therefore we compare the critical forces. The criterion used for the critical force in the experiment is the smallest force at which the normalized critical current

becomes smaller than 95% when the pressure is released. The criterion used for the critical force in the FE model is the smallest force at which the strain in the ReBCO layer reaches 0.45%.

The model contains three parts: the tape, the anvil and the pushing head (figure 25).

This geometry has plane symmetry therefore we model only half the geometry of the pushing head, anvil and tape. Note that the ReBCO layer of the tape is closer to the anvil.

The FE mesh for all parts is shown in figure 26. We use the C3D8R finite element instead of the recommended C3D20 because using C3D20 leads to bad convergence of the solver in some cases. For the tape we use three elements through the thickness for the copper, one for the ReBCO layer and five for the Hastelloy layer, approximately 70 elements for the width and 50 for the length. In reality the lateral sides of the tape are also covered of the copper but we not account this fact because it does not influence on the result. For the accurate solution, the mesh is biased near the edge of the pushing head in axial direction of the tape. The mesh for the pushing head and the anvil is also shown in figure 26. These parts also have a non-uniform mesh with higher density in the areas of expected stress concentration.

We define two contact pairs, one for the pushing head and the tape and the other for the anvil and the tape with 0.3 friction coefficient between the surfaces. We assume average value for the friction coefficient between metals. The symmetry boundary condition is defined on the respective faces of the anvil, pushing head and the tape. Also we apply the displacement boundary condition to the top of the pushing head, and the fixed boundary condition to the narrow side of the anvil (figure 26).

The material properties for the tape components are taken the same as for the tensile model. For the pushing head and anvil we use the elasto-plastic properties of stainless steel 316 at 77 K (table 7).

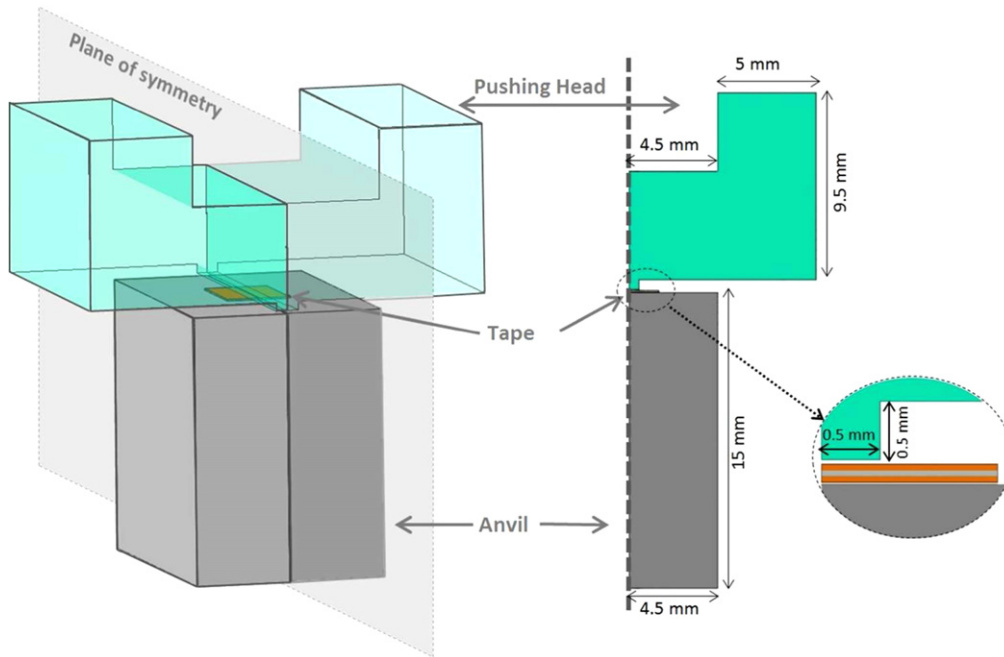


Figure 25. The assembly of the press setup, showing a piece of tape, anvil and pushing head by isometric view (left) and by side view (right).

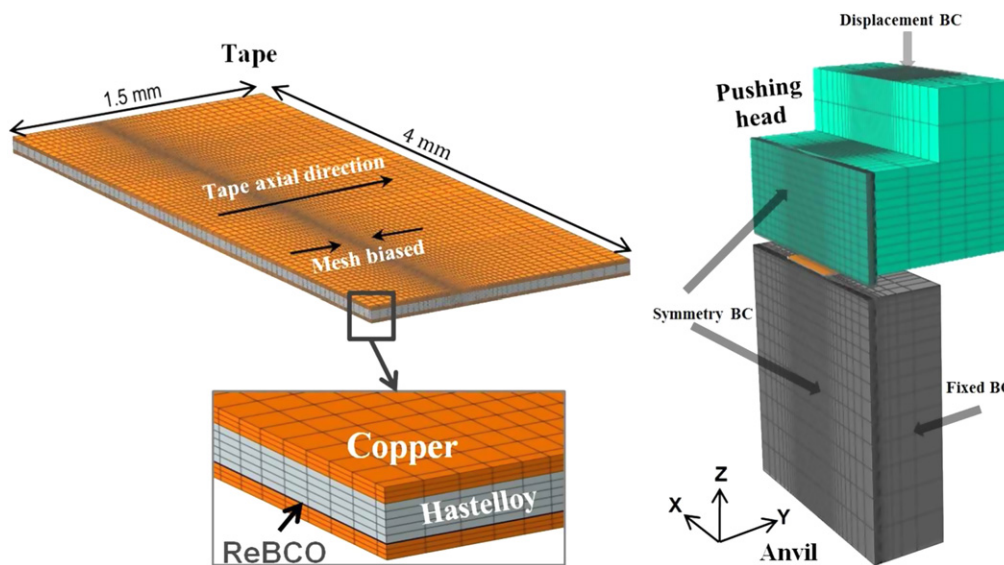


Figure 26. The FE mesh of the tape, anvil and pushing head, and boundary condition.

Table 7. Elasto-plastic properties of stainless steel 316 at 77 K [14, 15].

Young's modulus (GPa)	195
Poisson ratio	0.30
Yield stress (MPa)	1400
Ultimate tensile strength (MPa)	1790

The sequence of the FE model steps is the following: in the first two steps we model the production process of the tape (similarly to tensile or tensile-torsion model) and in the third step the pushing head moves down towards the anvil.

The calculations are done for the tapes with different thickness of the copper layer: 0, 40, 100 and 110 μm . For each

case we use an average of the authentic profile of the tape cross-section. The average profile is created from at least three cross-sections taken along the tape (figure 10). As a first result of the modeling, we obtain the critical force that is the reaction force of the pushing head along Z-axis at which the strain in the ReBCO layer reaches 0.45% at least in one element. These results and the critical force from the related experiments are listed in table 8.

We see that the critical force obtained from the experiments is about twice larger than from the modeling. This large difference shows that the criterion of 0.45% strain in a single element of the ReBCO layer is not appropriate for the transverse load. The reason for such a big difference is analogous to that found in the case of applied torsion; by using

Table 8. Critical force for the tapes with different copper thickness from the experiment and FE modeling using a criterion of 0.45% strain in a single element for FE model.

Tape type (copper thickness)	Critical force, kN		
	FEM	Experiment	Deviation, %
SF4050 (0 μm) ^a	1.76		
SCS4050 (40 μm)	1.42	3.02	53
SCS4050 (100 μm)	0.80	1.61	50
SCS4050 (110 μm)	0.73	1.29	44

^a The critical force was not reached in the experiment for this case.

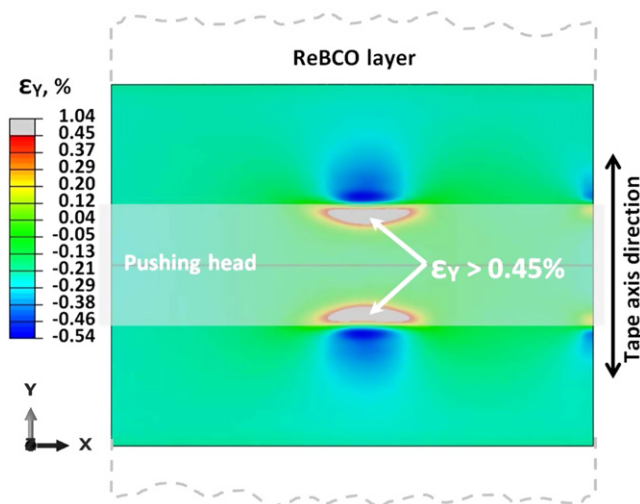


Figure 27. The longitudinal strain (along tape axis) in the ReBCO layer for SCS4050 tape with 100 μm copper for 1.3 kN pushing force obtained by FE modeling (top view). The area with the strain above 0.45% is about 0.7 mm across the tape or 17.5% of the tape width.

the 0.45%-criterion, we assume that the critical current begins to degrade irreversibly as soon as a strain of 0.45% is reached anywhere in the ReBCO layer. However, this little amount of damage may hardly affect the critical current at the $10 \mu\text{V m}^{-1}$ criterion, since the resulting increase in voltage at the same current is insignificant. We call the area in which the strain exceeds 0.45% the ‘damaged area’ because cracks appear in the superconducting ReBCO layer [5]. In reality the critical current begins to degrade when the damaged area occupies 15–20% of the width of the tape, this is illustrated in figure 27. To define the correct critical force we use a fit to the $I_c(\epsilon)$ relation of the tape as presented in figure 7, including the irreversible behavior at high tensile axial strain. Integrating the areas with different I_c of the ReBCO layer in the tape as depicted in figure 27, depending on the transverse pressure, allows calculating the degradation of the I_c depending on the axial strain state and damage of the ReBCO layer (I_c -integration method). Table 9 shows the critical force calculated by the combination of FEM and I_c -integration method and obtained experimentally.

The lesser difference of about 20% between model and experiment when using the I_c -integration method is already

Table 9. Critical force for the tapes with different copper thickness from experiment and combination of FEM and I_c -integration method.

Tape type with copper thickness	Critical force, kN		
	FEM + I_c -integration method	Experiment	Deviation, %
SF4050 (0 μm)	3.50	>3.45 ^a	
SCS4050 (40 μm)	2.40	3.02	21
SCS4050 (100 μm)	1.30	1.61	19
SCS4050 (110 μm)	1.10	1.29	15

^a The critical force was not reached in the experiment for this case.

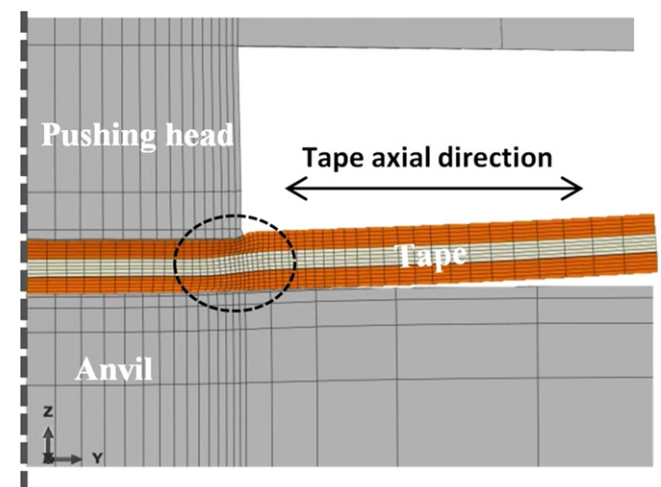


Figure 28. Calculated deformation of the tape, anvil and pushing head for SCS4050 tape with 100 μm copper under 1.3 kN of the pushing force (cross-section view).

much better than using the criterion of 0.45% strain in a single ReBCO finite element. This systematic deviation of smaller critical force in the FE model is not identified but is likely due to the assumptions required for the I_c -integration method and to less extent by experimental errors.

From figure 27 it can be seen that the areas with the peak strain are located in the middle of the tape and close to the pushing head edges. When the force is applied to the pushing head, there are two processes in the tape: one is the extrusion of the tape from under the pushing head and anvil and the other is bending of the tape at the edge of the pushing head (figure 28). This results in the peak longitudinal strain in the ReBCO layer near the edge of the pushing head. In combination with the non-uniform tape profile, this leads to isolated areas with peak strain. This result is confirmed by observation of cracks in the ReBCO layer by SEM (scanning electron microscope) method on samples after transverse load testing. On the SEM micrographs in figure 29 we see cracks in the ReBCO layer in the area near the edge of the pushing head (point 1) and no cracks near the center of the pushing head (point 2). The fact that we observe the peak strain and cracks

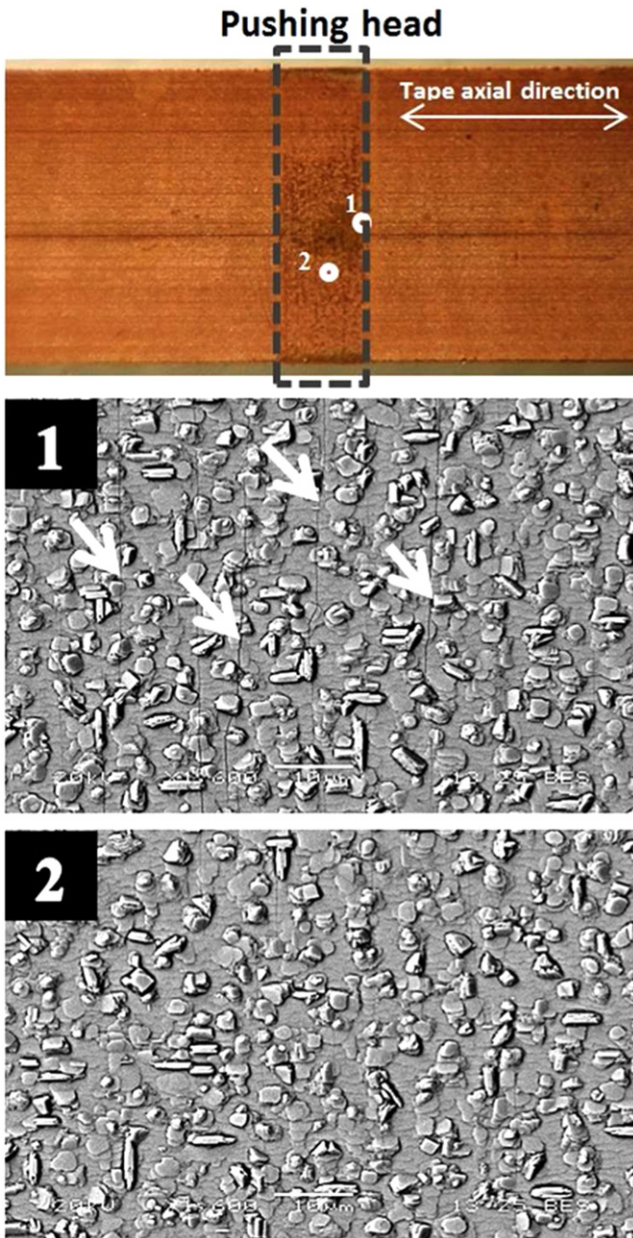


Figure 29. Observation of the ReBCO layer surface by SEM method after the transverse load experiment. (The white arrows shows the transverse cracks in the ReBCO layer).

in the axial centerline of the tape can be explained by the cross-sectional profile of the tape as shown in figure 10, with thicker copper layer in the center. The reason why the cracks appear at the edges of the pushing head as shown in figure 27 is because of the bending and plastic deformation of the copper layer, extruding more copper when moving away from the center of the pushing head and accumulating the in-plane strain in the ReBCO layer. This is illustrated in figure 28 with the highest in-plane strains in the elliptical striped zone.

The copper extrusion effect suggests that there is a relation between the copper plating thickness and critical force, although also the copper non-uniformity along the cross section width plays a role. Indeed, this dependency of the critical force on the thickness of the copper layer is

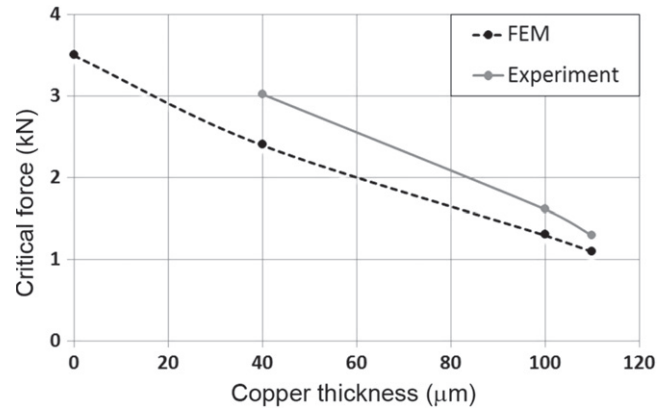


Figure 30. The critical force for the tapes versus different copper thickness obtained by FEM and experiment.

observed. The critical force decreases considerable with increase of the copper thickness with good agreement between FEM and experiment as shown in figure 30. A thick copper layer of about 100 μm reduces the critical force by factor 3, with respect to absence of a copper layer.

From these observations it is important to notice that performance improvement under applied load may be anticipated when avoiding the dog-boning effect, and creating a more uniform tape profile. Remarkably, in addition it is shown that the ‘copper extrusion effect’ causes lower critical force levels with increasing copper thickness, so a larger copper thickness does not act as a protection against mechanical load but reduces its performance potential.

Thus we can conclude that the combination of FE model and I_c -integration method for determination of the critical force is valid for the transverse load case. The criterion of 0.45% critical strain in the ReBCO layer is also appropriate in this case. However, for application of the model in cable and magnet design, an irreversibility limit of 0.45% for the strain remains crucial, since in any case damage to the ReBCO layer should be avoided. Arriving at this point, noticing satisfactory agreement between experiment and FE model for all loading cases studied so far, we find that the FE model can be used for cable modeling, for instance for CORC, twisted stack-tape or Roebel cable under manufacture and operating conditions.

5. Conclusion

New FE models for high temperature ReBCO superconducting tape subjected to tensile, a combination of tensile and torsional and transvers loads were presented in this paper. The models allow for calculating the critical loads at which the critical current begins to degrade irreversibly. The threshold criterion of 0.45% strain in the ReBCO layer as a starting point for irreversible critical current degradation is appropriate for all applied load types. For transverse load it is necessary to calculate the actual strain distribution in the ReBCO layer over the contact area and integrate the associated critical current to obtain the critical force, for torsion to less extend. It is necessary to use elasto-plastic properties of materials and include modeling of the production process of

the tape to achieve a good correlation with the experiments. The FE model allows understanding the mechanism of crack appearance especially for transverse load case. The critical force reduces considerably with increasing thickness of the copper layer, a factor three reduction is observed for 100 μm total copper layer thickness.

A performance improvement of electroplated copper ReBCO tape under applied load may be anticipated when the dog-boning is avoided, thus creating a more uniform tape profile and more homogeneous stress distribution. Moreover, the 'copper extrusion effect' under transverse load causes lower critical force levels with increasing copper thickness, so a larger copper thickness on the tape does not act as a protection against mechanical load when only in transverse direction but works opposite by reducing its performance potential.

Acknowledgments

The authors acknowledge SuperPower[®] for the kindly provided tape samples.

References

- [1] van der Laan D C 2009 $\text{YBa}_2\text{Cu}_3\text{O}_{7-\delta}$ coated conductor cabling for low ac-loss and high-field magnet applications *Supercond. Sci. Technol.* **22** 065013
- [2] Takayasu M, Mangiarotti F J, Chiesa L, Bromberg L and Minervini J V 2013 Conductor characterization of YBCO twisted stacked-tape cables *IEEE Trans. Appl. Supercond.* **23** 4800104
- [3] Goldacker W, Nast R, Kotzyba G, Schlachter S I, Frank A, Ringsdorf B, Schmidt C and Komarek P 2006 High current DyBCO-ROEBEL assembled coated conductor (RACC) *J. Phys.: Conf. Ser.* **43** 901–4
- [4] SuperPower[®] 2G HTS Wire Specifications (www.superpower-inc.com/system/files/SP_2G+Wire+Spec+Sheet_for+web_2012FEC_v2_1.pdf)
- [5] Osamura K, Sugano M, Machiya S, Adachi H, Ochiai S and Sato M 2009 Internal residual strain and critical current maximum of a surrounded Cu stabilized YBCO coated conductor *Supercond. Sci. Technol.* **22** 065001
- [6] Wessel S, Nijhuis A, Ilyin Y A, Abbas W, ten Haken B and ten Kate H H J 2004 A novel test arrangement for strain influence on strands (TARSIS): mechanical and electrical testing of ITER Nb3Sn strands *Adv. Cryog. Eng. Mater.* **50** 466–73
- [7] Godeke A, Dhalle M, Morelli A, Stobbelaar L, van Weeren H, van Eck H J N, Abbas W, Nijhuis A, den Ouden A and ten Haken B 2004 A device to investigate the axial strain dependence of the critical current density in superconductors *Rev. Sci. Instrum.* **75** 5112–8
- [8] ten Haken B, Godeke A and ten Kate H H J 1993 New devices for measuring the critical current in a tape as a function of the axial and transverse strain *IEEE Trans. Appl. Supercond.* **3** 1273–6
- [9] McLoughlin C, Thimont Y, Noudem J, Harnois C and Bernstein P 2012 The decrease of the critical current of coated conductors when a perpendicular magnetic field is applied: a Josephson effect point of view *Phys. Proc.* **36** 1564–9
- [10] Hazelton D 2011 *Application of SuperPower 2G HTS Wire to High Field Devices Presented at MT22 (France, Marseille, September 2011)*
- [11] Majkic G, Mensah R J and Selvamanickam V 2009 Electromechanical behavior of IBAD/MOCVD YBCO coated conductors subjected to torsion and tension loading *IEEE Trans. Appl. Supercond.* **19** 3003–8
- [12] Cheon J H, Shankar P S and Singh J P 2005 Influence of processing methods on residual stress evolution in coated conductors *Supercond. Sci. Technol.* **18** 142–6
- [13] Kalali A T and Hadidi-Moud S 2013 A semi-analytical approach to elastic-plastic stress analysis of FGM pressure vessels *J. Solid Mech.* **5** 63–73
- [14] Special Metals Corporation 2004 Publication Number SMC-019 (www.specialmetals.com/files/alloys/inconel/Inconel%20alloy%20C-276.pdf)
- [15] Iwasa Y 2009 *Case Studies in Superconducting Magnets Design and Operational Issues (Selected Topics in Superconductivity)* (Berlin: Springer)
- [16] Freund L B and Suresh S 2003 *Thin Film Materials: Stress, Defect Formation, and Surface Evolution* (Cambridge: Cambridge University Press)